Role of AI in Theranostics: Towards Routine Personalized Radiopharmaceutical Therapies

Julia Brosch-Lenz[1], Fereshteh Yousefirizi[1], Katherine Zukotynski[2], Jean-Mathieu Beauregard[3,4], Vincent Gaudet[5], Babak Saboury[6,7,8], Arman Rahmim[1,9,10], Carlos Uribe[10,11,*]

[1]Department of Integrative Oncology, BC Cancer Research Institute, Vancouver, BC, Canada
[2]Department of Medicine and Radiology, McMaster University, Hamilton, ON, Canada
[3]Department of Radiology and Nuclear Medicine, and Cancer Research Centre, Université Laval, Québec City, QC, Canada

[4]Department of Medical Imaging, and Research Center (Oncology Axis), CHU de Québec - Université Laval, Québec City, QC, Canada

[5]Department of Electrical and Computer Engineering, University of Waterloo, Waterloo, ON, Canada

[6]Department of Radiology and Imaging Sciences, Clinical Center, National Institutes of Health, Bethesda, MD, USA

[7]Department of Computer Science and Electrical Engineering, University of Maryland Baltimore County, Baltimore, MD, USA
[8]Department of Radiology, Hospital of the University of Pennsylvania, Philadelphia, PA, USA
[9]Department Physics, University of British Columbia, Vancouver, BC, Canada
[10]Department of Radiology, University of British Columbia, Vancouver, BC, Canada
[11]Department of Functional Imaging, BC Cancer, Vancouver, BC, Canada
*Corresponding author: curibe@bccrc.ca

Keywords: Theranostics; Radiopharmaceutical therapies; Dosimetry; Artificial intelligence; Outcome prediction; Segmentation; Registration; Quantitative Imaging

Key points:

1. AI has shown promising applications in quantitative imaging required for dosimetry.

2. Segmentation of organs and tumors, the most time consuming task in the dosimetry workflow, can be automated using AI.

3. Using the theranostic approach, AI models that predict absorbed dose and therapy outcomes might play a key role in personalizing RPTs.

4. AI has significant potential to improve accuracy and reduce times for routine implementation of patient-specific dosimetry in RPTs.

Disclosure statement: The authors have nothing to disclose.

Abstract

We highlight emerging uses of artificial intelligence (AI) in the field of theranostics, focusing on its significant potential to enable routine and reliable personalization of radiopharmaceutical therapies (RPTs). Personalized RPTs require patient-individual dosimetry calculations accompanying therapy. Image-based dosimetry needs: 1) quantitative imaging; 2) co-registration and organ/tumor identification on serial and multimodality images; 3) determination of the time-integrated activity; and 4) absorbed dose determination. AI models that facilitate these steps are reviewed. Additionally we discuss the potential to exploit biological information from diagnostic and therapeutic molecular images to derive biomarkers for absorbed dose and outcome prediction, towards personalization of therapies. We try to motivate the nuclear medicine community to expand and align efforts into making routine and reliable personalization of RPTs a reality.

Introduction

Radiopharmaceutical therapy (RPT) has shown promise in the treatment of various cancer types [1]. Metabolic processes or specific receptors serve as targets for the design of appropriate radiopharmaceuticals. The principle of "theranostics", in the context of nuclear medicine (Figure 1), uses pairs of radiopharmaceuticals to meet and explore both, therapeutic and diagnostic purposes (i.e. "thera-nostic"). The pharmaceuticals bind to the same target and can be radiolabeled with either a therapeutic (e.g. beta or alpha emitting) or diagnostic imaging (e.g. positron or gamma emitting) radionuclide [2]. This approach allows us to "see what we treat" and "treat what we see" at the molecular level.
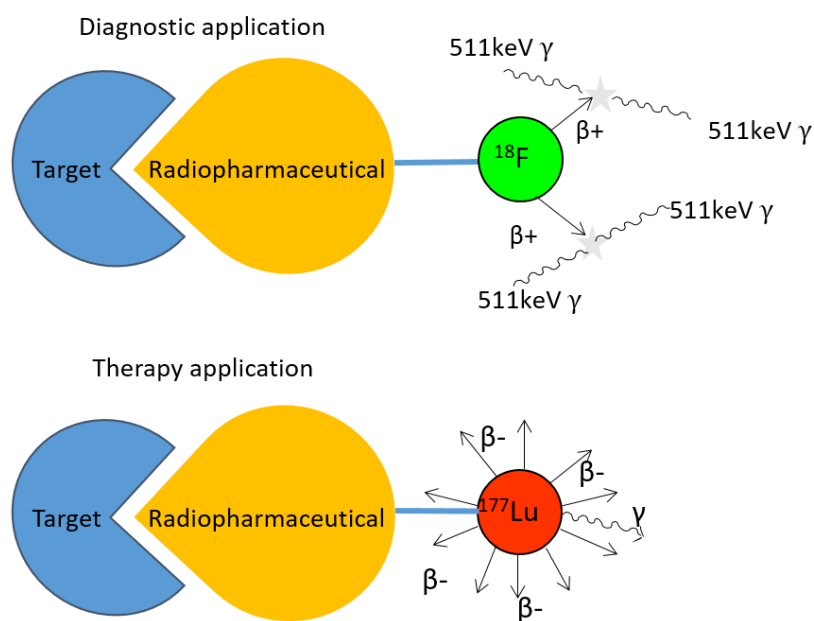
Figure 1: An example of the principle of theranostics in nuclear medicine. Here, a radiopharmaceutical (yellow) developed to bind to the target (blue) can be labeled both with Fluorine-18 (^{18}F) for diagnostic imaging purposes and Lutetium-177 for therapeutic procedures.

Two examples of recent radiopharmaceutical developments include targeting (i) the somatostatin receptors for the diagnosis and treatment of neuroendocrine tumors (NET) [3], and (ii) the prostate specific membrane antigen (PSMA) to diagnose and treat metastatic castration resistant prostate cancer (mCRPC) [4]. These are major frontiers in nuclear medicine, with significant existing and upcoming investments and efforts [5]. So far, the procedure guidelines from the International Atomic Energy Agency (IAEA), the Society of Nuclear Medicine and Molecular Imaging (SNMMI), and the European Association of Nuclear Medicine (EANM) have suggested the use of several cycles of a fixed therapeutic injection containing an activity of 7.4 GBq when Lutetium-177 (^{177}Lu) labelled compounds are used for NETs [6] or mCRPC treatments [7]. For NETs, [^{177}Lu]Lu-oxodotreotide has been approved by regulatory agencies to be used with a fixed activity of 7.4 GBq as the only option [8], and a similar framework is expected for [^{177}Lu]Lu-PSMA-617 for mCRPC in the near future.

Treatment planning, however, should consider individual factors such as the patient's weight and height, the tumor burden, overall patient's health condition as well as personal preferences and values. The organs at risk (OARs) tolerance to radiation and function as well as the patient-specific biological clearance and uptake of the radiopharmaceutical are further of substantial interest in personalized therapy. The key prerequisite for personalizing RPTs are routine and reliable dosimetry calculations. If dosimetry accompanies RPT, relationships between tumor and OAR radiation absorbed dose and therapy outcomes could be derived, providing evidence for adaptive treatment planning in clinical practice [9].

The present state of RPTs (Figure 2A) involves a diagnostic scan that is used by the physician to determine if a patient is suitable for therapy. If the patient expresses the target of interest, it is then referred to several cycles of therapy. Inter-therapy imaging is performed to qualitatively assess the performance of the treatment (e.g. to visualize distribution of the therapeutic radiopharmaceutical). To date, the use of routine post-therapy dosimetry has been hindered by its complexity and immense workload for physicians, technologists, and medical physicists. Thus, to be adopted into routine clinical practice, not only does the technique need to be accurate, but also practical. Any development that simplifies, automates, or accelerates the steps within the dosimetry workflow would be likely to increase implementation of personalized medicine. Artificial intelligence (AI) may be a game changer in supporting and facilitating the dosimetry workflow.
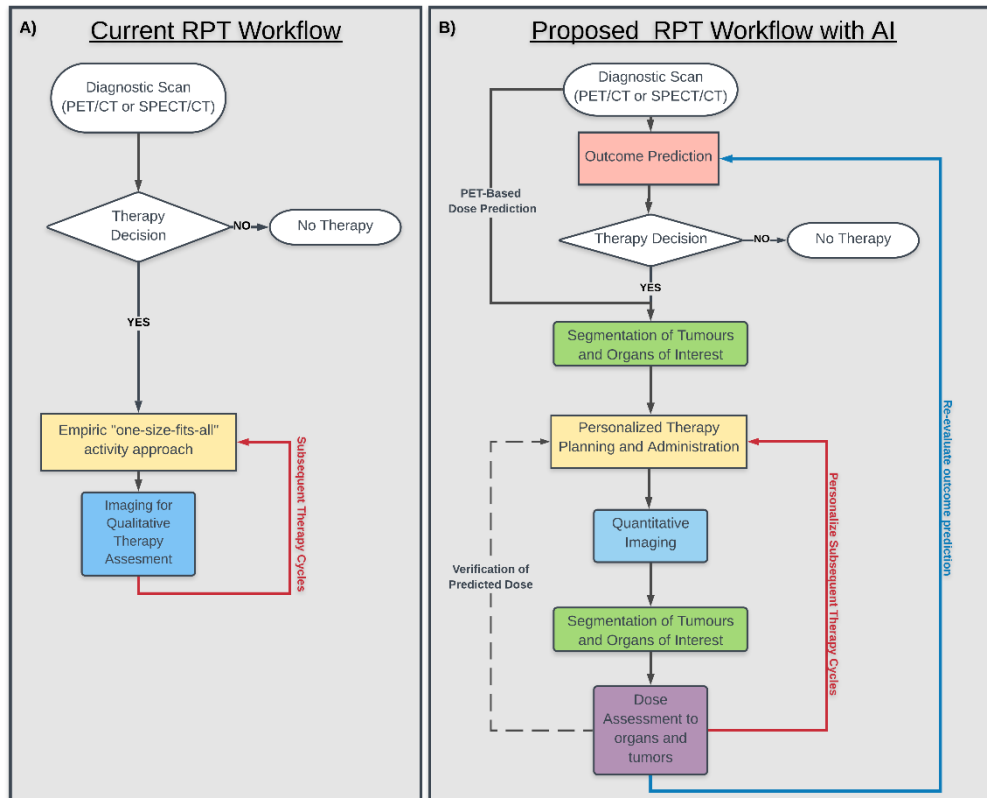
Figure 2: A) Current typical workflow of RPTs in which dosimetry is not routinely implemented. This only requires a diagnostic examination to establish the suitability of a patient for therapy and possibly qualitative images to determine how good or bad the treatment is performing. B) This diagram represents our vision for the whole theranostics approach. AI is a tool that can assist in every step in this workflow. Even more importantly, AI could predict outcomes and absorbed doses from pre-therapy diagnostic scans to personalize the treatment starting from the first cycle.

Our vision for a comprehensive theranostics framework (Figure 2B) involves the use of AI to simplify and motivate the personalization of RPTs. AI not only has direct applications in the different steps that form the dosimetry workflow (Figure 3), but could potentially be used to predict outcomes and absorbed doses.

In this work, we aim to highlight areas of importance on which AI can play a very significant role in dosimetry using the theranostics approach. First, we focus on the current challenges of dosimetry after the administration of the therapeutic radiopharmaceutical and discuss the related AI applications. Later, we describe our

view on how AI can move us towards personalized RPTs making the theranostics workflow proposed in Figure 2B a reality.

Image-based dosimetry in RPTs

The goal of internal dosimetry is to assess the radiation dose absorbed in healthy and malignant tissue. Report 85 of the International Commission on Radiation Units and Measurements (ICRU) [10] defines absorbed dose caused by the interactions of ionizing radiation in organs and tumors as the amount of energy deposited per unit mass of tissue.

The Committee on Medical Internal Radiation Dose (MIRD) has defined guidelines to estimate absorbed dose in RPT using quantitative images acquired at different time points following administration of a therapeutic radiopharmaceutical [11]. These images are used to measure the radiopharmaceutical biodistribution over time [12]. The workflow for image-based dosimetry includes several processing steps [13] that are illustrated in Figure 3 and correspond to the same colored boxes of Figure 2B. Below, we discuss each of the different steps required for accurate absorbed dose assessments and make recommendations on how AI can further assist throughout the workflow.

Figure 3

Figure 3 Schematic representation of the dosimetry workflow for any image-based absorbed dose estimation for radiopharmaceutical therapy.

The role of AI in quantitative imaging

The first step in the dosimetry workflow (Figure 3) is the acquisition of quantitative images that allow for the accurate measurement of activity [14]. The goal is to measure the biodistribution of the radiotracer as a function of time. The number of imaging time points that should be acquired is a compromise between optimization of resources, simplification of protocols, and the accuracy for which the patient-specific effective half-life of the radiopharmaceutical can be estimated [15]. Quantitative imaging also implies the use of standardized acquisition protocols, image reconstruction parameters, and methods to determine the camera calibration factor [11, 16].

Both, single photon emission computed tomography (SPECT) and positron emission tomography (PET), are quantitative imaging modalities that allow us to measure radioactivity distribution in the patient over time. Image acquisition and reconstruction parameters needed for accurate quantification is a topic of ongoing research.

Recent work has assessed the reduction in the number of acquired SPECT projections to reduce scan time without compromising quantitative accuracy or image quality. Rydén et al. [17] used a deep convolutional U-net-shaped neural network to generate intermediate ^{177}Lu SPECT projections (i.e. projections that were not acquired). They found that adding the projections generated by the U-net to the sparsely acquired projections provided similar visual image quality compared to the reference of a full set of projection data. Furthermore, they found comparable kidney activity concentration compared to the one measured from the reconstructed image using a full set of projections. The main advantage of this method is that it allows to scan patients in a much shorter acquisition time. Other investigations have suggested

the reduction in acquisition time per projection or the total number of acquired projections in myocardial perfusion SPECT may be compensated for using a deep residual neural network [18].

AI has also been used to generate quantitative images with PET. Studies involving less injected activity or faster acquisitions have been performed [19-21].

Other studies have focused on improvements in image reconstruction [22-26]. Image degrading effects such as scatter and attenuation need to be corrected for to obtain quantitative images. Scatter correction remains a challenging task in SPECT reconstruction, especially for the imaging of pure-beta emitters that do not create any gamma emissions in their decay chain (e.g. Yttrium-90). In these scenarios, the detected energy spectrum of the photons corresponds to the Bremsstrahlung photons. Xiang et al. [27] used Monte Carlo (MC) simulated phantom data to create projections and understand the scatter components. They used this dataset to train a deep convolutional neural network (CNN) that estimated the scatter component in the projections. The CNN estimated scatter was compared to the one derived from MC simulations. The results were very similar between MC and CNN with the advantage that the latter required only a mere fraction of time compared to MC. The use of a fully connected CNN for SPECT reconstruction was investigated by Shao et al. [28] and outperformed conventional ordered subset expectation maximization (OSEM) SPECT reconstruction in terms of image resolution and quantitation.

In PET, new state-of-the-art reconstruction algorithms such as the block sequential regularized expectation maximization algorithm (BSREM) allow for a higher number of iterations without amplifying the image noise [29]. However, the increased number of iterations also increases the time needed to generate an image. AI has been

used to speed up the reconstruction by generating images for intermediate iterations [30]. The improvements of reconstruction of newly introduced total body PET images using deep learning (DL) methods is subject to ongoing research [31].

Image denoising allows for the reconstruction of quantitative images with less injected activity, faster acquisition times, or with a higher number of iterations in the reconstruction algorithm. There have been studies showing denoising methods using AI CNNs with scintillation cameras data [32], using generative adversarial networks (GAN) [33] for PET, and using coupled U-Nets for SPECT [34].

The interest in targeted alpha therapies [35] is rapidly increasing, though the quantitative imaging remains a challenge [36]. AI methods could be applied to improve both, image quantification accuracy and quality.

The role of AI in image registration and segmentation

The positioning of the patient during pre- and post-therapy scans is highly variable. To match the different organs and tumors' radiopharmaceutical uptake between imaging points, accurate image registration is required (Figure 2 and Figure 3). Moreover, anatomical changes (e.g. tumor shrinking or disease progress) between time points requires non-rigid registration methods to fully account for those changes.

Multi-modality and multi-time point registration

Medical image registration is necessary for subsequent segmentation, treatment planning, image-guided radiotherapy and response assessment [37]. Different imaging modalities such as magnetic resonance (MR), computed tomography (CT), PET and SPECT exhibit differences in resolution and provide different complementary information (i.e. anatomical vs. functional). In addition to discrepancies

of patient positioning, intra-abdominal organ movement can occur between the CT and the PET or SPECT acquisition within a single examination. Co-registration of serial and multi-modality images, however, is a challenging task within the dosimetry workflow.

Conventional registration techniques such as rigid, non-rigid [38] and multiresolution approaches [39] can be used for this task. Since image deformation may lead to changes in organ/tumor volumes, that get reflected in mass and activity measurements, it has a direct impact on the estimated absorbed dose. The registration method must be chosen and validated carefully. Significant differences have been shown in absorbed dose estimates, depending on whether manual, rigid or deformable registration methods are applied [38].

AI techniques have shown better accuracy and robustness compared to conventional registration methods and can be generalized better across different modalities [40]. Moreover, AI approaches can mitigate the effects of image artifacts on registration results [41]. Despite the fact that most AI-based registration techniques have not been developed specifically for RPT applications, they have the potential to support the radiation therapy workflow [42].

DL using CNNs has been used for medical image registration using supervised and unsupervised schemes. For instance, supervised training of a convolutional stacked auto-encoder was proposed by Wu et al. [40] to learn discriminative features of images from different modalities. These features were then used in iterative deformable registration.

An unsupervised AI-based registration method was proposed by de Vos et al. [43] and Shan et al. [44] using a CNN without the need to include ground truth labels. Liao et al. [45] proposed a method based on CNNs and reinforcement learning for CT

to cone-beam CT registration. Studies on synthetic images (using GANs) with known labels to train a deep registration model without the need of annotated data also exist [46]. A 3D unsupervised network that utilizes a metabolic constraint function (MCF) and a multi-modal similarity measure for PET/CT image registration was proposed by Yu et al. [47] (Figure 4). The MCF is defined based on the standard uptake value (SUV) distribution of hypermetabolic regions to reduce the distortion on the displacement vector field (DVF). The DVF is estimated using a 3D CNN. 3D PET images are then wrapped to 3D CT images by a spatial transformer. The spatial and frequency domain similarity is then calculated based on the registered PET patches and the original CT patches. The loss function of the registration framework is the weighted sum of spatial and frequency similarity and a smoothness of DVF. A similar architecture could potentially be applied to the SPECT/CT data acquired during therapy (Figure 2) and to register diagnostic PET images to the therapeutic images.
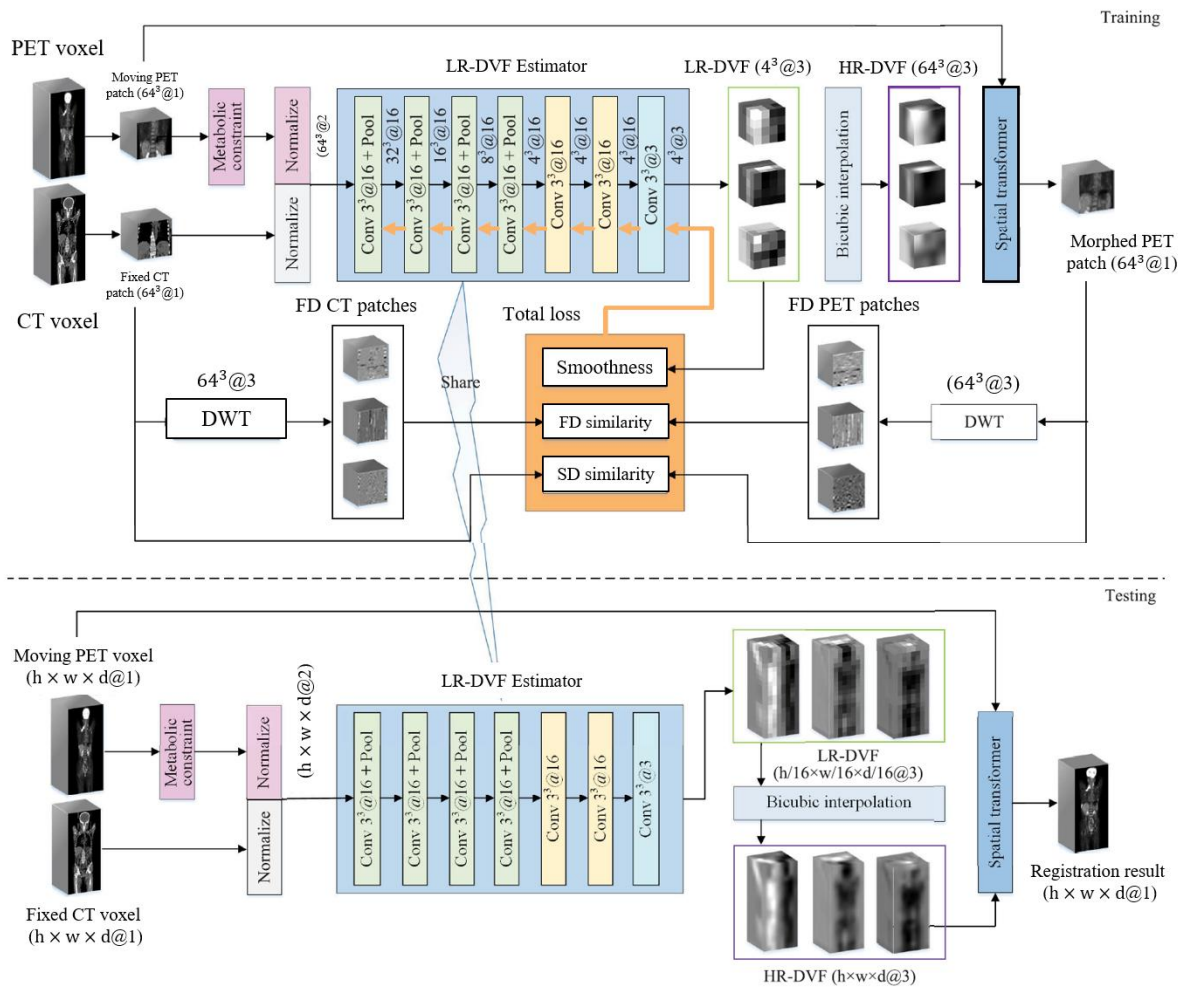
Figure 4: The unsupervised 3D registration framework proposed by Yu et al. [47]. The figure has already been published under the Creative Commons License which allows us to redistribute it in this document. A copy of the license can be found in https://creativecommons.org/licenses/by/4.0.

Recent investigations by Guerra et al. [48] for radioembolization purposes used two different CNNs for automatic liver segmentation on MR and CT images respectively, and subsequently registered the segmentation results. We hypothesize that these AI approaches can be used in the future in a RPT context with multiple time point multi-modality images by using CNNs for segmentation and subsequent VOI co-registration.

Segmentation of organs and tumors

The identification of OARs and tumors on images is important for absorbed dose

estimation. The segmentation of tumors is required for tumor dosimetry that is a critical component in determining the treatment response of RPT [49]. However, segmentation is the most time-consuming task in the dosimetry workflow (Figure 2 and Figure 3) since it often relies on manual delineation of volumes of interest (VOI) [50-52]. Segmentation allows the measurement of activity within each organ and tumor as well as the estimate of the corresponding mass of each VOI. Both quantities are required for accurate dosimetry calculations.

Compared to external beam radiotherapy, it is even more challenging for manual segmentation of tumor lesions for RPT, which specifically treats patients with metastatic cancer. Often patients may have a large number of lesions across the body, of heterogeneous sizes and tracer uptakes. Segmentation of all these lesions manually is not practical. Manual segmentation is also subject to intra- [53] and inter-observer variability [54]. Validated AI-based models for fully automated, robust, accurate segmentation of organs/lesions in PET, PET/CT and SPECT/CT images can help delineate OARs and lesions to achieve a personalized dosimetry framework. Normal organ segmentation approaches using DL models could use CT data [55, 56], or combined image data such as PET/CT [57, 58]. Wang et al. [59] segmented normal organs based on CT images using a multi-atlas method and refined the segmentation on the PET images. A triple-combining 2.5D U-Net, which simultaneously extracts features from axial, coronal and sagittal planes, has been developed to mimic the workflow of physicians for the automated characterization of lesions on PSMA PET [60].

Diagnostic PET images can be expected to have similar intensity profiles as SPECT images acquired in therapy because they are targeting the same receptors. This allows using transfer-learning approaches for segmentation. Diagnostic PET

images should be smoothed in this regard to account for the differences in resolution with respect to SPECT. The quality of CT images is the same or very similar between PET/CT and SPECT/CT modalities. AI models can be pre-trained on PET/CT images and then "tuned" using SPECT/CT data. The cross-modality knowledge transfer for lesion segmentation in SPECT images using PET segmentations can be done using unsupervised adversarial training to learn feature mapping between domains (PET and SPECT) as previously shown for domain adaptation from MR to CT [61]. The Probability map (PM) based on diagnostic PET images can be estimated and added to the segmentation model for SPECT/CT images. This learnt PM captures the probability that a voxel in a SPECT image belongs to a tumor or OAR. The PM may not be accurate enough to fully segment SPECT/CT images (as tumors can change over time) but can be used as initial guidance (e.g. increase probability of detection for smaller tumors).

In the direct context of segmentation for dosimetry, Jackson et al. [62] showed promising results when using a 3D CNN for kidney segmentation on the low-dose CT from post-therapy [^{177}Lu]Lu-PSMA SPECT/CT against manual organ delineation for renal absorbed dose estimation. In addition, a 3D U-net model was proposed for kidney segmentation for uptake quantification [63]. Tang et al. [64] suggested a CNN model for liver segmentation be used for personalized liver radioembolization.

Besides intra-therapy cycle image registration and segmentation, the possibility to transfer VOIs to subsequent cycles should be investigated. AI could further assist in registering and segmenting intra-abdominal organ movement and tumor shrinkage or disease progress between therapy cycles.

The role of AI in time activity curve assessment and time-integration of activity

Following registration and segmentation, the next step of the dosimetry workflow pertains to the fit of a model function to the time activity curve (TAC) (Figure 3) on an organ or voxel level. This model function must be chosen carefully to describe the pharmacokinetics of the radiopharmaceutical under investigation. Typically, mono-exponential or bi-exponential functions are used (Figure 5) but tri-exponential functions have also been found in literature [65]. Also, there are situations in which the initial uptake is approximated using a trapezoid. The subsequent calculation of the time-integrated activity (TIA) can be performed on an organ or voxel level. The latter yields a 3D time-integrated activity map (TIAM) [66], from which a 3D absorbed dose estimation can be completed.
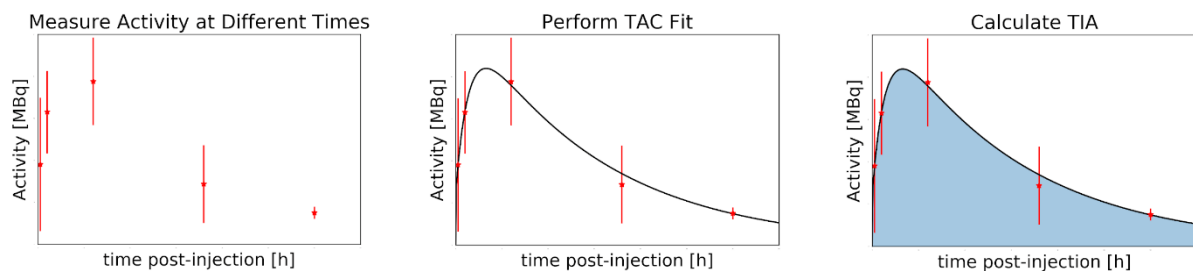

Figure 5 Simplified representation of the derivation of TIA: Measurement of activity over time at discrete points; fit of mono-exponential decay function to data points; calculation of the area under the curve, i.e. time-integrated activity.

The fit function describes the pharmacokinetics of the radiopharmaceutical. Sarrut et al. [66] described a multimodal fitting approach on the voxel level for multiple fitting models using nonlinear least square optimization. The best fitting model per voxel was then chosen based on the Akaike information criterion similar to the proposed one in the NUKFIT software by Kletting et al. [67]. The applicability of a particle filter to denoise TACs on the voxel level was proposed by Götz et al. [68] with promising results. Kost et al. [69] on the contrary used a different approach of first

generating absorbed dose rate maps on each of the serial quantitative activity images at the voxel level followed by pharmacokinetic modelling.

AI remains to be actively used for TAC or TIA estimation with great potential in this step of the dosimetry workflow both in organ or voxel level approaches. Possible applications could include investigation of CNNs that use information of serial quantitative images to predict TIAs using only a single post-therapy scan. Moreover, data from the diagnostic imaging could be used in conjunction with the single therapeutic image acquisition to improve the TAC and thus have higher confidence in the absorbed dose results further down the workflow. Lastly, AI can use the information from the diagnostic scans and therapeutic cycles together to improve the TIA of subsequent therapy cycles. Reducing the number of post-therapy scans is advantageous for the patients' comfort and decreases the workload for clinical personnel. Advances in image co-registration and reconstruction may further enhance progress in minimizing error from voxel-wise fitting due to image artifacts in individual voxels.

The role of AI in conversion to absorbed dose

The last step of the workflow entails the conversion of TIA into absorbed dose (Figure 3). Dosimetry can be performed on an organ [70] or voxel level [71, 72], each associated with different degrees of accuracy and complexity.

Organ level absorbed dose estimation according to MIRD [70] uses organ- and radionuclide specific S-values derived from simulations with reference human phantoms. These S-values yield the absorbed dose in a target organ per decay in a source organ. The radiation absorbed dose to an organ is hence derived from the sum of all sources to target combinations of TIAs multiplied by the respective S-values.

Similarly, voxel S-value kernels are simulated for a specific tissue composition and radionuclide. Kernels are then convolved with the TIAM to create 3D absorbed dose maps [71]. Monte Carlo (MC) simulations use the patient-individual 3D CT and TIAM to precisely model the absorbed dose for heterogeneous tissues and activity distributions [72]. Whilst MC simulation-based dosimetry taking into account heterogeneous activity and tissue distributions is still the gold standard against to which other methods are validated [73, 74], this is the most complex, computationally demanding and time-consuming dosimetry method. AI offers the potential to maintain accuracy of MC dosimetry while reducing the time required. Table 1 summarizes the different assumptions made when different dosimetry approaches are used.

When using / Type of	Organ S-value	Voxel S-value	MC dosimetry simulation
Activity distribution	Homogeneous	Heterogeneous	Heterogeneous
Tissue composition	Homogeneous medium	Homogeneous medium	Heterogeneous patient anatomy using CT
Dose Output	Mean absorbed dose	3D absorbed dose map	3D absorbed dose map

Table 1: Different assumptions per dosimetry method and yielded absorbed dose result (i.e. organ or voxel level). The complexity as well as the accuracy of dosimetry methods increases from left to right.

Image-based organ or voxel level dosimetry approaches yield macroscopic absorbed doses. However, there is increasing interest in describing the radiation damage on smaller region of an organ or tumor or even at the cellular level [75]. Knowing this can provide a better understanding of the underlying radiobiological effects during RPT [76-78]. Currently, RPTs are limited to absorbed doses based on the experience of external beam radiation therapies (EBRT). However, differences in absorbed dose rates and number of cycles of RPT compared to EBRT has lead us to think that different absorbed dose limits should be set for internal radiation therapies. As an example, the absorbed dose to kidneys is commonly limited to 23 Gy. However, absorbed doses of up to 40 Gy have been shown to be tolerated by patients without risk factors [79]. AI can potentially be used to combine multi-scale dosimetry knowledge

for accurate effective dose modeling. AI may unveil the complex relationship between pre-therapy patient data, such as imaging, demographic data, lab results, and the radiation dose distribution to be obtained during therapy, which is a problem too complicated to be described by conventional mathematical modelling approaches. GANs attempt to model the post-therapy voxel-wise dosimetry directly from pre-therapy imaging.

The prediction of deposited energy distribution and voxel-based dosimetry using a deep neural network was assessed by Akhavanallaf et al. [51] as illustrated in Figure 6. Their approach used whole-body 3D density maps (derived from patient CT images) and 3D absorbed dose maps (generated with MC simulations) as input to train a deep neural network to generate tissue-specific S-value kernels. Their method has the potential to overcome the general limitation of voxel S-value kernels that assume homogenous tissue and typically water density. Götz et al. [80] used a CNN to predict density specific voxel S-value kernels.

As alternative to MC dosimetry, Lee et al. [81] studied the use of a CNN for dosimetry estimation at a voxel level. Their network was trained to yield absorbed dose rate maps for activity and tissue distributions of Gallium-68 (^{68}Ga) [^{68}Ga]Ga-NOTARGD PET/CT based on ground truth MC simulation derived absorbed dose rate maps. The dose difference of CNN derived absorbed dose rate maps against MC was below 2% with a time-effort of less than 4 minutes compared to over 235 hours computation time of the MC simulation. Similarly, Götz et al. [82] trained a CNN with MC reference absorbed dose maps to generate voxel absorbed dose maps on the input of density maps from CT and TIAMs from serial ^{177}Lu SPECT/CT. The predicted absorbed dose maps from the model outperformed the use of a soft tissue voxel S-value kernel when compared to MC generated absorbed dose maps.

Step 1: Specific S-value kernel prediction

Random sampled (central voxel)

CT image batch (64*64*64)

13 Segmented medium

Dose distribution Kernel (64*64*64)

Step 2: Patient-specific dose map calculation

Density map

Central source $(voxel_k)$

$S(voxel_k \leftarrow voxel_n)$

Activity map

WB dose map

$$\bar{D}_{voxel_k} = \sum_{n=1}^{N} \tilde{A}_{voxel_n} \cdot S(voxel_k \leftarrow voxel_n)$$
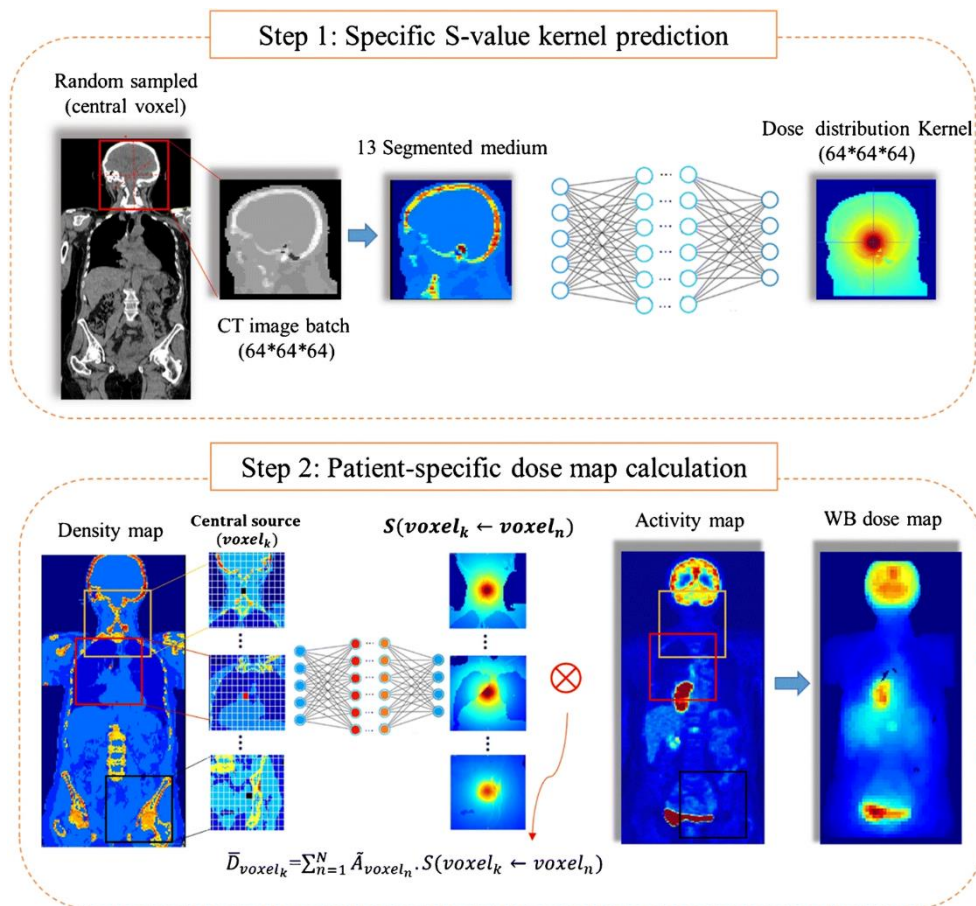
Figure 6: Diagram of the procedure used by Akhavanallaf et. al. [51] in which a dose kernel is generated using a deep neural network. The kernel can then be convolved with the TIAM to generate an absorbed dose distribution. The figure has been already published under the Creative Commons Attribution 4.0 that allows us to redistribute it in this document. A copy of the license can be found in https://creativecommons.org/licenses/by/4.0.

AI and the future of personalized RPT: radiomics, dosiomics and outcome prediction

Improved therapeutic absorbed dose estimation directly translates into the possibility of correlating absorbed dose with tumor response or normal organ toxicities. Knowledge of absorbed dose-response relationships might enable us to personalize activity planning for subsequent therapy cycles. Combined analysis of diagnostic imaging and therapeutic radiation absorbed doses might then allow for therapy outcome prediction.

Because of the theranostics approach, the outcome prediction could potentially be implemented with the diagnostic scans even before the RPT. This prediction can then be verified and updated in combination with additional information collected in

subsequent therapy cycles (Figure 2B). Studies like the one performed by Xue et al. [83] have already used voxel-wise absorbed dose prediction for [^{177}Lu]Lu-PSMA therapy based on pre-therapeutic PSMA PET/CT. They trained GANs using the diagnostic [^{68}Ga]Ga-PSMA PET/CTs and 3D absorbed dose maps. This described approach in combination with known dose-response relationships could assist the physicians in making the best therapy decision (Figure 2B). AI has shown the capability to discover effective predictive biomarkers for treatment outcome and long-term survival. There is an untapped potential to apply radiomics analysis to molecular imaging (both from pre- and post-therapy images) that can contain biological information. Moreover, there might be features detectable from within the 3D absorbed dose maps that can also show value towards better understanding of therapy response and outcome, enabling further personalization of therapies. We refer to the analysis performed on the 3D absorbed dose maps using the term dosiomics. The combination of radiomic features from CT, PET, MRI, and SPECT with dosiomic features from the absorbed dose maps can be used to train AI models that can better guide physicians with treatment planning and absorbed dose predictions. Moreover, deep learning approaches using different modalities of imaging and absorbed dose maps can inherently find features that are good predictors of outcome.

To develop robust outcome prediction models based on radiomics and dosiomics, the datasets must be representative of the disease and contain variant types and severities of it. Standardized imaging protocols and pre-processing steps are important to ensure consistent image quality [84]. An array of features can be used as input to the models for outcome prediction. For example, (i) absorbed dose-volume histogram measures could be computed from segmented 3D absorbed dose maps and are increasingly available in radiomics software packages. Such measures could also

be correlated with tumor control probability and potential normal tissue toxicity. (ii) Quantitative features from diagnostic scans such as SUV_{mean}, SUV_{max}, SUV_{peak}, molecular tumor volume, total lesion activity (TLA), and total lesion fraction (i.e. TLA divided by body weight) could further serve as input for outcome prediction models. Analysis can be performed using PET-only, SPECT-only, and PET/SPECT. The subtraction of these parameters between cycles could be applied for outcome prediction [85, 86]. (iii) The analysis can include an array of radiomics features, beyond the above-mentioned simpler metrics. It has been shown that radiomic features at PET resolution can preserve their value at lower SPECT resolution [87].

Investigations can include the detection of radiomic features in relation to biomarkers for disease staging [88] and could be extended to use of neural networks (NNs) or CNNs to predict the outcome of therapy [89-91]. In addition, NNs can model nonlinear survival data by classifications [92]. A deep network can directly extract and identify the most predictive radiomic features and could further learn unique features that may not be captured by handcrafted radiomics. The new paradigms of fusion radiomics, have been investigated on PET/CT in head & neck cancer [93, 94] and could be extended to SPECT/CT scans. Furthermore, subsequent therapy cycles could involve adapted therapy planning based on available dosimetry and outcome modeling.

As technology keeps improving, it also expands the possibilities of data collection. For example, recently developed total body PET scanners [95, 96] would enable the collection of dynamic whole-body data [97, 98] of the diagnostic radiopharmaceutical. This allows for the generation of parametric images that also provide information about the biokinetics of the radiopharmaceutical [99]. Although there are limitations related to the early acquisition time and shorter half-life of diagnostic radionuclides compared to therapeutic radionuclides, AI can play an

important role in understanding the dynamic scans and can possibly predict the uptake of the radiopharmaceutical in the therapy cycle.

In addition, the denoising examples mentioned before, in combination with more sensitive scanners, can allow us to perform the diagnostic scan at much later times that might correspond to the washout phase of the radiotracer. For example, it has been reported that the new EXPLORER total body PET scanner has the ability to image a patient injected with [^{18}F]FDG up to 5 half-lives after injection [96]; something unthinkable with current limited axial field of view scanners. Also, longer half-life PET radionuclides such as Copper-64 (^{64}Cu) (12.7 h half-life) or Zirconium-89 (^{89}Zr) (78.4 h half-life) that are used to label theranostic pairs, could provide the data required to predict absorbed doses and outcomes for which AI is a fantastic tool to explore with currently existing scanners.

Benefiting of the emerging research and applications of AI in the fields of quantitative imaging, segmentation, registration absorbed dose prediction, and outcome modelling we believe personalized therapies can easily be implemented in the clinical setting.

Conclusion

For adaptive RPT planning and personalized activity prescription, predictive dosimetry prior to treatment as well as absorbed dose verification is required to optimize therapy. For that, it is mandatory to have standardized protocols and reliable absorbed dose values first. Hence, efforts should concentrate on accuracy improvements of any of the steps within the dosimetry workflow. Cancer treatments are often difficult and complex, but the nuclear medicine community can incorporate the technological advancements of AI to make dosimetry a feasible task in the clinical

setting. This includes applications for image quantification, registration, segmentation, biodistribution modeling, and absorbed dose value calculation. Predictive modelling of therapy outcome and absorbed doses following a therapeutic injection can assist in treatment planning and benefit patients from personalized RPTs.

The future of personalized radiopharmaceutical therapy will likely benefit from active utilization of AI methods in the field of theranostics. This work highlighted different possible applications of AI, with the hope to motivate the community to expand and align efforts towards routine and reliable personalization of RPTs.

List of Abbreviations

AI: Artificial intelligence

BSREM: Block sequential regularized expectation maximization algorithm

CNN: Convolutional neural network

CT: Computed tomography

^{64}Cu: Copper-64

DL: Deep learning

DVF: Displacement vector field

EANM: European association of nuclear medicine

EBRT: External beam radiation therapy

^{18}F: Fluorine-18

GAN: Generative adversarial network

IAEA: International atomic energy agency

ICRU: International commission on radiation units and measurements

^{177}Lu: Lutetium-177

MC: Monte carlo

MCF: Metabolic constraint function

mCRPC: Metastatic, castration-resistant prostate cancer

MIRD: Medical internal radiation dose

MR: Magnetic resonance

NET: Neuroendocrine tumor

NN: Neural network

OAR: Organ at risk

OSEM: Ordered subset expectation maximization

PET: Positron emission tomography

PM: Probability map

PSMA: Prostate-specific membrane antigen

RPT: Radiopharmaceutical therapy

SNMMI: Society of nuclear medicine and molecular imaging

SPECT: Single photon emission computed tomography

SUV: Standard uptake value

TAC: Time activity curve

TIA: Time-integrated activity

TIAM: Time-integrated activity map

TLA: Total lesion activity

VOI: Volume of interest

References

1. Sgouros, G., et al., *Radiopharmaceutical therapy in cancer: clinical advances and challenges.* Nature Reviews Drug Discovery, 2020. **19**(9): p. 589-608.
2. Yordanova, A., et al., *Theranostics in nuclear medicine practice.* OncoTargets and therapy, 2017. **10**: p. 4821.

3. Kaemmerer, D., et al., *Molecular imaging with 68 Ga-SSTR PET/CT and correlation to immunohistochemistry of somatostatin receptors in neuroendocrine tumours.* European journal of nuclear medicine and molecular imaging, 2011. **38**(9): p. 1659.

4. Benešová, M., et al., *Preclinical evaluation of a tailor-made DOTA-conjugated PSMA inhibitor with optimized linker moiety for imaging and endoradiotherapy of prostate cancer.* Journal of Nuclear Medicine, 2015. **56**(6): p. 914-920.

5. Herrmann, K., et al., *Radiotheranostics: a roadmap for future development.* The Lancet Oncology, 2020. **21**(3): p. e146-e156.

6. Zaknun, J.J., et al., *The joint IAEA, EANM, and SNMMI practical guidance on peptide receptor radionuclide therapy (PRRNT) in neuroendocrine tumours.* European journal of nuclear medicine and molecular imaging, 2013. **40**(5): p. 800-816.

7. Kratochwil, C., et al., *EANM procedure guidelines for radionuclide therapy with 177 Lu-labelled PSMA-ligands (177 Lu-PSMA-RLT).* European journal of nuclear medicine and molecular imaging, 2019. **46**(12): p. 2536-2544.

8. Strosberg, J., et al., *Phase 3 trial of 177Lu-Dotatate for midgut neuroendocrine tumors.* New England Journal of Medicine, 2017. **376**(2): p. 125-135.

9. Strigari, L., et al., *The evidence base for the use of internal dosimetry in the clinical practice of molecular radiotherapy.* European journal of nuclear medicine and molecular imaging, 2014. **41**(10): p. 1976-1988.

10. Seltzer, S., et al., *ICRU report 85 fundamental quantities and units for ionizing radiation.* J. ICRU, 2011. **11**(1).

11. Dewaraja, Y.K., et al., *MIRD pamphlet no. 23: quantitative SPECT for patient-specific 3-dimensional dosimetry in internal radionuclide therapy.* Journal of Nuclear Medicine, 2012. **53**(8): p. 1310-1325.

12. Sgouros, G., et al. *Three-dimensional imaging-based radiobiological dosimetry.* in *Seminars in nuclear medicine.* 2008. Elsevier.

13. Mora-Ramirez, E., et al., *Comparison of commercial dosimetric software platforms in patients treated with 177Lu-DOTATATE for peptide receptor radionuclide therapy.* Medical Physics, 2020. **47**(9): p. 4602-4615.

14. Li, T., et al., *Quantitative imaging for targeted radionuclide therapy dosimetry-technical review.* Theranostics, 2017. **7**(18): p. 4551.

15. Siegel, J.A., et al., *MIRD pamphlet no. 16: techniques for quantitative radiopharmaceutical biodistribution data acquisition and analysis for use in human radiation dose estimates.* Journal of Nuclear Medicine, 1999. **40**(2): p. 37S-61S.

16. Uribe, C.F., et al., *Accuracy of 177 Lu activity quantification in SPECT imaging: a phantom study.* EJNMMI physics, 2017. **4**(1): p. 1-20.

17. Rydén, T., et al., *Deep-Learning Generation of Synthetic Intermediate Projections Improves 177Lu SPECT Images Reconstructed with Sparsely Acquired Projections.* Journal of Nuclear Medicine, 2021. **62**(4): p. 528-535.

18. Shiri, I., et al., *Standard SPECT myocardial perfusion estimation from half-time acquisitions using deep convolutional residual neural networks.* Journal of Nuclear Cardiology, 2020: p. 1-19.

19. Katsari, K., et al., *Artificial intelligence for reduced dose 18F-FDG PET examinations: a real-world deployment through a standardized framework and business case assessment.* EJNMMI physics, 2021. **8**(1): p. 1-15.

20. Xiang, L., et al., *Deep auto-context convolutional neural networks for standard-dose PET image estimation from low-dose PET/MRI.* Neurocomputing, 2017. **267**: p. 406-416.

21. Le, V., et al., *Effect of PET Scan with Count Reduction Using AI-Based Processing Techniques on Image Quality.* Journal of Nuclear Medicine, 2020. **61**(supplement 1): p. 3095-3095.

22. Wang, T., et al., *Machine learning in quantitative PET: A review of attenuation correction and low-count image reconstruction methods.* Physica Medica, 2020. **76**: p. 294-306.

23. Shi, L., et al., *Deep learning-based attenuation map generation for myocardial perfusion SPECT.* European Journal of Nuclear Medicine and Molecular Imaging, 2020: p. 1-13.

24. Hwang, D., et al., *Generation of PET attenuation map for whole-body time-of-flight 18F-FDG PET/MRI using a deep neural network trained with simultaneously reconstructed activity and attenuation maps.* Journal of Nuclear Medicine, 2019. **60**(8): p. 1183-1189.

25. Shiri, I., et al., *Deep-JASC: joint attenuation and scatter correction in whole-body 18 F-FDG PET using a deep residual network.* European journal of nuclear medicine and molecular imaging, 2020. **47**: p. 2533-2548.

26. Dietze, M.M., et al., *Accelerated SPECT image reconstruction with FBP and an image enhancement convolutional neural network.* EJNMMI physics, 2019. **6**(1): p. 1-12.

27. Xiang, H., et al., *A deep neural network for fast and accurate scatter estimation in quantitative SPECT/CT under challenging scatter conditions.* European journal of nuclear medicine and molecular imaging, 2020: p. 1-12.

28. Shao, W., M.G. Pomper, and Y. Du, *A learned reconstruction network for SPECT imaging.* IEEE transactions on radiation and plasma medical sciences, 2020. **5**(1): p. 26-34.

29. Ahn, S., et al., *Quantitative comparison of OSEM and penalized likelihood image reconstruction using relative difference penalties for clinical PET.* Physics in Medicine & Biology, 2015. **60**(15): p. 5733.

30. Cheng, L., et al. *Accelerated iterative image reconstruction using a deep learning based leapfrogging strategy.* in *International conference on fully three-dimensional image reconstruction in radiology and nuclear medicine.* 2017.

31. Ma, R., et al., *Total-Body PET Images Reconstruction Optimization Using Deep Learning.* Nuklearmedizin, 2021. **60**(02): p. V45.

32. Minarik, D., O. Enqvist, and E. Trägårdh, *Denoising of scintillation camera images using a deep convolutional neural network: a Monte Carlo simulation approach.* Journal of Nuclear Medicine, 2020. **61**(2): p. 298-303.

33. Wang, Y., et al., *3D conditional generative adversarial networks for high-quality PET image estimation at low dose.* Neuroimage, 2018. **174**: p. 550-562.

34. Liu, J., et al., *Deep learning with noise-to-noise training for denoising in SPECT myocardial perfusion imaging.* Medical Physics, 2021. **48**(1): p. 156-168.

35. Yadav, M.P., et al., *Efficacy and safety of 225Ac-PSMA-617 targeted alpha therapy in metastatic castration-resistant Prostate Cancer patients.* Theranostics, 2020. **10**(20): p. 9364.

36. Gosewisch, A., et al., *Image-based dosimetry for 225 Ac-PSMA-I&T therapy using quantitative SPECT.* European journal of nuclear medicine and molecular imaging, 2021. **48**(4): p. 1260-1261.

37. Brock, K.K., et al., *Use of image registration and fusion algorithms and techniques in radiotherapy: Report of the AAPM Radiation Therapy Committee Task Group No. 132.* Medical physics, 2017. **44**(7): p. e43-e76.

38. Grassi, E., et al., *Effect of image registration on 3D absorbed dose calculations in 177Lu-DOTATOC peptide receptor radionuclide therapy.* Physica Medica, 2018. **45**: p. 177-185.

39. Dandois, F., et al., *SCreg: a registration-based platform to compare unicondylar knee arthroplasty SPECT/CT scans.* BMC musculoskeletal disorders, 2020. **21**(1): p. 1-8.

40. Wu, G., et al., *Scalable high-performance image registration framework by unsupervised deep feature representations learning.* IEEE Transactions on Biomedical Engineering, 2015. **63**(7): p. 1505-1516.

41. Huynh, E., et al., *Artificial intelligence in radiation oncology.* Nature Reviews Clinical Oncology, 2020. **17**(12): p. 771-781.

42. Kearney, V., et al., *An unsupervised convolutional neural network-based algorithm for deformable image registration.* Physics in Medicine & Biology, 2018. **63**(18): p. 185017.

43. de Vos, B.D., et al., *End-to-end unsupervised deformable image registration with a convolutional neural network*, in *Deep learning in medical image analysis and multimodal learning for clinical decision support.* 2017, Springer. p. 204-212.

44. Shan, S., et al., *Unsupervised end-to-end learning for deformable medical image registration.* arXiv preprint arXiv:1711.08608, 2017.

45. Liao, R., et al. *An artificial agent for robust image registration.* in *Proceedings of the AAAI Conference on Artificial Intelligence.* 2017.

46. Mahapatra, D., et al. *Deformable medical image registration using generative adversarial networks.* in *2018 IEEE 15th International Symposium on Biomedical Imaging (ISBI 2018).* 2018. IEEE.

47. Yu, H., et al., *Unsupervised 3D PET-CT Image Registration Method Using a Metabolic Constraint Function and a Multi-Domain Similarity Measure.* IEEE Access, 2020. **8**: p. 63077-63089.

48. Guerra, J., et al., *Novel Low-Dose CT based Automatic Segmentation and Registration Framework for Liver Radioembolization Planning.* Nuklearmedizin, 2021. **60**(02): p. P38.

49. Violet, J., et al., *Dosimetry of (177)Lu-PSMA-617 in Metastatic Castration-Resistant Prostate Cancer: Correlations Between Pretherapeutic Imaging and Whole-Body Tumor Dosimetry with Treatment Outcomes.* J Nucl Med, 2019. **60**(4): p. 517-523.

50. Lee, M.S., et al., *Whole-body voxel-based personalized dosimetry: the multiple voxel S-value approach for heterogeneous media with nonuniform activity distributions.* Journal of Nuclear Medicine, 2018. **59**(7): p. 1133-1139.

51. Akhavanallaf, A., et al., *Whole-body voxel-based internal dosimetry using deep learning.* European Journal of Nuclear Medicine and Molecular Imaging, 2021. **48**(3): p. 670-682.

52. Vinod, S.K., et al., *Uncertainties in volume delineation in radiation oncology: a systematic review and recommendations for future studies.* Radiotherapy and Oncology, 2016. **121**(2): p. 169-179.

53. Starmans, M.P., et al., *Radiomics: data mining using quantitative medical image features*, in *Handbook of Medical Image Computing and Computer Assisted Intervention.* 2020, Elsevier. p. 429-456.

54. Gudi, S., et al., *Interobserver variability in the delineation of gross tumour volume and specified organs-at-risk during IMRT for head and neck cancers and the impact of FDG-PET/CT on such variability at the primary site.* Journal of medical imaging and radiation sciences, 2017. **48**(2): p. 184-192.

55.   Bieth, M., et al., *Segmentation of skeleton and organs in whole-body CT images via iterative trilateration.* IEEE transactions on medical imaging, 2017. **36**(11): p. 2276-2286.

56.   Yu, Y., et al., *3D lymphoma segmentation in PET/CT images based on fully connected CRFs*, in *Molecular Imaging, Reconstruction and Analysis of Moving Body Organs, and Stroke Imaging and Treatment.* 2017, Springer. p. 3-12.

57.   Xu, L., et al., *Automated Whole-Body Bone Lesion Detection for Multiple Myeloma on 68Ga-Pentixafor PET/CT Imaging Using Deep Learning Methods.* Contrast Media Mol Imaging, 2018. **2018**: p. 11.

58.   Hu, X., et al., *Coarse-to-Fine Adversarial Networks and Zone-based Uncertainty Analysis for NK/T-cell Lymphoma Segmentation in CT/PET images.* IEEE J Biomed Health Inform, 2020.

59.   Wang, H., et al., *Dual-modality multi-atlas segmentation of torso organs from [18 F] FDG-PET/CT images.* International journal of computer assisted radiology and surgery, 2019. **14**(3): p. 473-482.

60.   Zhao, Y., et al., *Deep neural network for automatic characterization of lesions on (68)Ga-PSMA-11 PET/CT.* Eur J Nucl Med Mol Imaging, 2020. **47**(3): p. 603-613.

61.   Dou, Q., et al., *Unsupervised cross-modality domain adaptation of convnets for biomedical image segmentations with adversarial loss.* arXiv preprint arXiv:1804.10916, 2018.

62.   Jackson, P., et al., *Deep learning renal segmentation for fully automated radiation dose estimation in unsealed source therapy.* Frontiers in oncology, 2018. **8**: p. 215.

63.   Ryden, T., et al., *Deep learning-based SPECT/CT quantification of 177Lu uptake in the kidneys.* Journal of Nuclear Medicine, 2020. **61**(supplement 1): p. 1401-1401.

64.   Tang, X., et al., *Whole liver segmentation based on deep learning and manual adjustment for clinical use in SIRT.* European journal of nuclear medicine and molecular imaging, 2020. **47**(12): p. 2742-2752.

65.   Jackson, P.A., et al., *An automated voxelized dosimetry tool for radionuclide therapy based on serial quantitative SPECT/CT imaging.* Medical physics, 2013. **40**(11): p. 112503.

66.   Sarrut, D., et al., *Voxel-based multimodel fitting method for modeling time activity curves in SPECT images.* Medical physics, 2017. **44**(12): p. 6280-6288.

67.   Kletting, P., et al., *Molecular radiotherapy: the NUKFIT software for calculating the time-integrated activity coefficient.* Medical physics, 2013. **40**(10): p. 102504.

68.   Götz, T.I., et al., *Particle filter de-noising of voxel-specific time-activity-curves in personalized 177Lu therapy.* Zeitschrift für Medizinische Physik, 2020. **30**(2): p. 116-134.

69.   Kost, S.D., et al., *VIDA: a voxel-based dosimetry method for targeted radionuclide therapy using Geant4.* Cancer Biotherapy and Radiopharmaceuticals, 2015. **30**(1): p. 16-26.

70.   Snyder, W., et al., *MIRD pamphlet no. 11.* The Society of Nuclear Medicine, New York, 1975: p. 92-93.

71.   Bolch, W.E., et al., *MIRD pamphlet no. 17: the dosimetry of nonuniform activity distributions—radionuclide S values at the voxel level.* Journal of Nuclear Medicine, 1999. **40**(1): p. 11S-36S.

72.   Sarrut, D., et al., *A review of the use and potential of the GATE Monte Carlo simulation code for radiation therapy and dosimetry applications.* Medical physics, 2014. **41**(6Part1).

73.   Brosch-Lenz, J., et al., *Influence of dosimetry method on bone lesion absorbed dose estimates in PSMA therapy: application to mCRPC patients receiving Lu-177-PSMA-I&T.* EJNMMI physics, 2021. **8**(1): p. 1-17.

74.   Dieudonné, A., et al., *Study of the impact of tissue density heterogeneities on 3-dimensional abdominal dosimetry: comparison between dose kernel convolution and direct Monte Carlo methods.* Journal of Nuclear Medicine, 2013. **54**(2): p. 236-243.

75.   Hobbs, R.F., et al., *A nephron-based model of the kidneys for macro-to-micro α-particle dosimetry.* Physics in Medicine & Biology, 2012. **57**(13): p. 4403.

76.   Vaziri, B., et al., *MIRD pamphlet no. 25: MIRDcell V2. 0 software tool for dosimetric analysis of biologic response of multicellular populations.* Journal of Nuclear Medicine, 2014. **55**(9): p. 1557-1564.

77.   Lampe, N., et al., *Mechanistic DNA damage simulations in Geant4-DNA part 1: A parameter study in a simplified geometry.* Physica Medica, 2018. **48**: p. 135-145.

78.   Alcocer-Ávila, M.E., et al., *Radiation doses from 161 Tb and 177 Lu in single tumour cells and micrometastases.* EJNMMI physics, 2020. **7**: p. 1-9.

79.   Bodei, L., et al., *Long-term evaluation of renal toxicity after peptide receptor radionuclide therapy with 90 Y-DOTATOC and 177 Lu-DOTATATE: the role of associated risk factors.* European journal of nuclear medicine and molecular imaging, 2008. **35**(10): p. 1847-1856.

80.   Götz, T.I., et al., *Dose voxel kernel prediction with neural networks for radiation dose estimation.* Zeitschrift für Medizinische Physik, 2021. **31**(1): p. 23-36.

81.   Lee, M.S., et al., *Deep-dose: a voxel dose estimation method using deep convolutional neural network for personalized internal dosimetry.* Scientific reports, 2019. **9**(1): p. 1-9.

82.   Götz, T.I., et al., *A deep learning approach to radiation dose estimation.* Physics in Medicine & Biology, 2020. **65**(3): p. 035007.

83.   Xue, S., et al., *Voxel-wise Prediction of Post-therapy Dosimetry for 177Lu-PSMA I&T Therapy using Deep Learning.* Journal of Nuclear Medicine, 2020. **61**(supplement 1): p. 1424-1424.

84.   Fournier, L., et al., *Incorporating radiomics into clinical trials: expert consensus endorsed by the European Society of Radiology on considerations for data-driven compared to biologically driven quantitative biomarkers.* European radiology, 2021: p. 1-12.

85.   Beauregard, J.-M., et al., *Development of Theranostic response criteria in solid tumors (THERCIST) and tumor burden quantification methods for 68Ga-PET/CT and 177Lu-QSPECT/CT.* Journal of Nuclear Medicine, 2019. **60**(supplement 1): p. 626-626.

86.   Beauregard, J.-M., et al., *Quantitative 177Lu-SPECT (QSPECT) during second cycle predicts 68Ga-octreotate-PET/CT molecular response to 177Lu-octreotate PRRT.* Journal of Nuclear Medicine, 2020. **61**(supplement 1): p. 411-411.

87.   Blinder, S.A., et al. *Texture and shape analysis on high and low spatial resolution emission images.* in *2014 IEEE Nuclear Science Symposium and Medical Imaging Conference (NSS/MIC).* 2014. IEEE.

88. Klyuzhin, I.S., et al., *Use of generative disease models for analysis and selection of radiomic features in PET.* IEEE Transactions on Radiation and Plasma Medical Sciences, 2018. **3**(2): p. 178-191.

89. Ypsilantis, P.-P., et al., *Predicting response to neoadjuvant chemotherapy with PET imaging using convolutional neural networks.* PloS one, 2015. **10**(9): p. e0137036.

90. Amyar, A., et al., *3-d rpet-net: development of a 3-d pet imaging convolutional neural network for radiomics analysis and outcome prediction.* IEEE Transactions on Radiation and Plasma Medical Sciences, 2019. **3**(2): p. 225-231.

91. Baek, S., et al., *Deep segmentation networks predict survival of non-small cell lung cancer.* Scientific reports, 2019. **9**(1): p. 1-10.

92. Katzman, J.L., et al., *DeepSurv: personalized treatment recommender system using a Cox proportional hazards deep neural network.* BMC medical research methodology, 2018. **18**(1): p. 1-12.

93. Lv, W., et al., *Multi-level multi-modality fusion radiomics: application to PET and CT imaging for prognostication of head and neck cancer.* IEEE journal of biomedical and health informatics, 2019. **24**(8): p. 2268-2277.

94. Lv, W., et al., *Radiomics analysis of PET and CT components of PET/CT imaging integrated with clinical parameters: application to prognosis for nasopharyngeal carcinoma.* Molecular imaging and biology, 2019. **21**(5): p. 954-964.

95. Cherry, S.R., et al., *Total-body PET: maximizing sensitivity to create new opportunities for clinical research and patient care.* Journal of Nuclear Medicine, 2018. **59**(1): p. 3-12.

96. Badawi, R.D., et al., *First human imaging studies with the EXPLORER total-body PET scanner.* Journal of Nuclear Medicine, 2019. **60**(3): p. 299-303.

97. Vandenberghe, S., P. Moskal, and J.S. Karp, *State of the art in total body PET.* EJNMMI physics, 2020. **7**: p. 1-33.

98. Zhang, X., et al., *First pre-clinical study of total-body dynamic PET imaging using the mini-EXPLORER scanner.* Journal of Nuclear Medicine, 2017. **58**(supplement 1): p. 394-394.

99. Wang, G., A. Rahmim, and R.N. Gunn, *PET Parametric Imaging: Past, Present, and Future.* IEEE Transactions on Radiation and Plasma Medical Sciences, 2020. **4**(6): p. 663-675.